SEMARAK ILMU PUBLISHING

CFD Letters

Journal homepage:
https://semarakilmu.com.my/journals/index.php/CFD_Letters/index
ISSN: 2180-1363

Analysis and Prediction of Equivalent Diameter of Air Bubbles Rising in Water

Gabriel de Carvalho Nascimento[1], Roger Matsumoto Moreira[2], Felipe Pereira de Moura[3], William Alves Tavares[4], Thiago Ferreira Bernardes Bento[5], Lorena Brandão Calazan[6,*], Milena Silva Andrade[6], Beatriz Freitas Rezende[1]

[1] Agricultural and Environmental Engineering Department, Engineering School, Federal Fluminense University, 24210-240 Niterói, Rio de Janeiro, Brazil
[2] Technical Drawing Department, Engineering School, Federal Fluminense University, 24210-240 Niterói, Rio de Janeiro, Brazil
[3] Institute of Chemistry, Federal Fluminense University, 24210-240 Niterói, Rio de Janeiro, Brazil
[4] Engineering School, Federal Fluminense University, 24210-240 Niterói, Rio de Janeiro, Brazil
[5] Mechanical Engineering Department, Federal Center for Technological Education, 20271-110 Rio de Janeiro, Rio de Janeiro, Brazil
[6] Civil Engineering, Engineering School, Federal Fluminense University, 24210-240 Niterói, Rio de Janeiro, Brazil

ARTICLE INFO

Article history:
Received 17 September 2023
Received in revised form19 October 2023
Accepted 20 November 2023
Available online 31 March 2024

Keywords:
Air bubbles; equivalent diameter; orifice inner diameter; flow rate; subsea leakage

ABSTRACT

The equivalent diameter of rising bubbles in liquids is an important parameter that has been investigated for decades by researchers for different purposes. Bubble diameter plays important role in quantifying oil and gas leaks in subsea leak analysis, since it allows the prediction of the magnitude of leaks in seabed petroleum wells and other structures through images obtained by underwater vehicles at great depths. Most studies available in the literature on the subject focus on investigating air bubbles in water; therefore, they were used as the main guide of the experimental apparatus described in this article. Several tests were conducted with air bubble chain in tap water, whose flow rate ranged from 21.1 mL/min to 234.4 mL/min, whereas the bubble equivalent diameter ranged from 4.1 mm to 8.2 mm. In addition, computational fluid dynamics simulations were carried out for comparison purposes; they were validated as potential tools to help designing an automated subsea gas leakage monitoring system based on image analysis algorithms. The herein proposed model could be both analytically and experimentally validated, based on comparisons to findings reported by other authors. This procedure enabled gathering evidence about the most efficient analytical predictions available in the literature for the herein addressed scenario. The results in the present study are consistent to those recorded in the main related articles.

1. Introduction

Several industrial processes are based on multiphase systems of bubbles rising in liquids, in the Chemistry, Petrochemistry, Biochemistry and Metallurgy fields [1]. This system is applied in processes such as aeration, flotation, fermentation control, microbiological growth, gasification, reagents'

* *Corresponding author.*
E-mail address: lorenabrandao@id.uff.br (Lorena Brandão Calazan)

https://doi.org/10.37934/cfdl.16.8.3347

addition, catalysis and induced agitation [2-4]. It is used due to excellent mixing, momentum, mass and heat transfer features [4-8]. In addition to industrial processes, gas leakage in subsea wells and pipelines is another important system that has high financial and environmental costs.

Many researchers have investigated rising bubble volume and its associated parameters. The concept of equivalent diameter is often adopted in studies about this topic. Equivalent diameter is defined as the diameter equivalent to a perfect sphere diameter of equal volume; it is expressed by the sphere volume equation:

$$V_b = \frac{\pi d_e^3}{6} \tag{1}$$

Here d_e is the bubble equivalent diameter and V_b is the bubble volume.

The first substantial progress in predicting bubble volume was achieved in 1864, based on the association among specific mass differential, $\Delta\rho = \rho_l - \rho_g$, gravity acceleration, g, capillary inner diameter, d_o, and interfacial tension of both fluids, σ. A traction factor was also used to correct contact angles other than 90° [9].

Tate [9] has justified his study based on medical prescriptions for non-standardized drops of medicines. Although his study addressed drops of liquids, it was widely applied to gas bubbles. However, this approach is used under quasi-static conditions, at extremely low flow rates [10].

Many authors have developed equations to predict the equivalent diameter of bubbles and drops; they were applied to different scenarios and fluid properties. The main equations available in the literature were selected and divided into those that take into consideration the flow rate, *Q*, and the ones that use dimensionless parameters.

Flow rate sometimes appears as a single parameter in equations used to calculate equivalent diameter; it is only necessary to adjust the range of different physical properties of fluids to the application scenario of each equation (Table 1). Orifice superficial velocity, u_o, is the ratio between flow rate and orifice inner area; therefore, it is an alternative parameter used for flow rate analysis.

Dimensionless parameters are often used to calculate bubble equivalent diameter. Overall, they are based on fluids' properties; sometimes, they are also linked to terminal velocity. Those presented here refer to Bond number (*Bd*), Eotvos number (*Eo*), Froude number (*Fr*), Galileo number (*Ga*) and Reynolds number (*Re*), which consist of the main dimensionless numbers regarding fluid dynamics (Table 2).

Experimental systems are often prepared in laboratory environment to investigate bubble formation, shape, aspect ratio, equivalent diameter and velocity [19-27]. Overall, these experiments comprise a tank filled with working liquid, the injection orifice at the bottom of it, the injection system and a camera.

The width and length of the tank must be sufficiently high to be an infinite wall problem, without wall interference. The height dimension can vary from 30 [25] to 200 cm [23] and it depends on both the technique and parameters to be used in the experiment.

The injection system mostly comprises syringes [21, 22, 25, 26] or cylinders [19, 20, 27]. In some cases, there is a bulkhead above the orifice's outlet to enable the production of larger bubbles [19, 20, 28]. Both the inner diameter of the orifice and the experimental bubble equivalent diameter investigated by the authors presented diversified magnitude of range (Table 3).

Table 1
Equations used to calculate d_e through Q

Reference	Equation
Van Krevelen and Hoftijzer [11]	$d_e = \left(1.722 \times \frac{6}{\pi} \times \frac{Q^{\frac{5}{6}}}{g^{\frac{3}{5}}}\right)^{\frac{1}{3}}$
Davidson and Schuler [12]	$d_e = \left(1.378 \times \frac{6}{\pi} \times \frac{Q^{\frac{5}{6}}}{g^{\frac{3}{5}}}\right)^{\frac{1}{3}}$
Davidson and Harrison [13]	$d_e = \left(1.138 \times \frac{6}{\pi} \times \frac{Q^{\frac{5}{6}}}{g^{\frac{3}{5}}}\right)^{\frac{1}{3}}$
Kumar and Kullor [14]	$d_e = \left(0.976 \times \frac{6}{\pi} \times \frac{Q^{\frac{5}{6}}}{g^{\frac{3}{5}}}\right)^{\frac{1}{3}}$
Akita and Yoshida [15]	$d_e = 1.88 \times d_o \times \left(\frac{u_o}{\sqrt{g \times d_o}}\right)^{\frac{1}{3}}$
Gaddis and Vogelpohl [16]	$d_e = \left[\left(\frac{6 \times \sigma \times d_o}{\rho \times g}\right)^{\frac{4}{3}} + \left(\frac{81 \times Q \times \upsilon}{\pi \times g}\right) + \left(\frac{135 \times Q^2}{4 \times g \times \pi^2}\right)^{\frac{4}{5}}\right]^{\frac{1}{4}}$

Table 2
Equations used to calculate d_e through dimensionless parameters

Author	Equation
Tate [9]	$d_e = \left(\frac{f \times \pi \times \sigma \times d_o}{\Delta\rho \times g}\right)^{\frac{1}{3}}$
Jamialahmadi [17]	$d_e = d_o \left[\frac{5}{Bd^{1.008}} + \left(\frac{9.26 Fr^{0.36}}{Ga^{0.39}}\right) + 2.147 \times Fr^{0.51}\right]^{\frac{1}{3}}$
Shi [10]	$d_e = 1.82 \times \left(\frac{d_o}{Eo^{\frac{1}{3}}}\right)$
Xiao [18]	$d_e = d_o \left(1.82 + \left(\frac{1.4773 Re_g Ra}{20691.2238\left(Re_g Ra\right)^{0.05242} + \left(\frac{Ra Re_g}{Re_l}\right)^2}, 1.2815\right) + 0.02218 Re_l^{-0.4771} Re_g^{0.9952} Eo^{-0.0008095}\right) E$

Table 3
Range of d_o and experimental d_e per authors

Author	d_e (mm)	d_o (mm)
Haberman and Morton [19]	0.4 - 20	-
Marks [20]	1.2 - 19	-
Tomiyama *et al.,* [22]	0.6 – 5.5	0.51, 0.9, 1.45 and 3.19
Wu and Gharib [21]	1 -2	0.27 – 0.44
Shew *et al.,* [23]	1.74 – 2.4	0.3
Liu *et al.,* [25]	0.54 – 10.2	0.6 – 7.7
Sharaf *et al.,* [26]	1.4 – 26.7	0.6
Wang and Socolofsky [27]	4.4 – 5.7	4.0

One, or more, cameras are positioned to capture images of the fluid-fluid system in photo and/or video format [18-28]. A source of light is often used behind the tank in order to refine bubbles' sharpness and to improve the quality of the image [18, 19, 24-28].

As previously mentioned, several scholars performed experimental tests focused on analyzing different air bubble parameters. However, only Wang and Socolofsky [27] performed tests with chain

air bubbles in tap water. Another similarity between the aforementioned study and the present research lies on the performance of tests with flow rate variation for the same orifice inner diameter. This experimental model makes it possible to evaluate the behavior of bubble equivalent diameter with the flow rate. Thus, Wang and Socolofsky [27] study was selected as the best experimental methodology available in the literature to be compared to the herein adopted methodology (Table 4).

Table 4
Experimental results reported by Wang and Socolofsky [27] (d_o = 4 mm)

Experimental test	Q (mL/min)	d_e (mm)
1	2.8	5.2
2	9.1	5.1
3	11.5	5.2
4	13.7	5.4
5	16.5	4.4
6	29.4	5.1
7	38.4	5.0
8	48.8	5.3
9	56.9	5.5
10	65.8	5.6
11	76.2	5.7

Therefore, the current study has analyzed the equivalent diameter of air bubbles rising in water and their association with both orifice inner diameter and flow rate, by comparing its results to those reported in the literature, based on a theoretical experimental assumption. Through the correlation between bubble equivalent diameter, orifice inner diameter and flow rate, it will be possible to advance significantly in the prediction of the magnitude of leaks in seabed pipelines and other structures through images obtained by underwater vehicles at great depths.

2. Methodology

2.1 Experimental Apparatus and Procedures

The herein used experimental apparatus comprised a glass tank filled with tap water, at room temperature (25°C) and pressure of 1 atm. Tank height was 400 mm; it presented rectangular cross section of 400 x 600 mm, which was enough to neglect the wall effects [29].

The gas injection system comprised an air compressor, a cylinder and a rigid plastic tube, which was connected to the tank through a hole in its side wall (Figure 1). The cylinder accounted for stabilizing any air flow intermittence. The voltage regulator, which enabled variations in flow rate, was connected to the injection system by a voltage stabilizer, whose function lied on limiting voltage variations and on avoiding damages to the compressor.

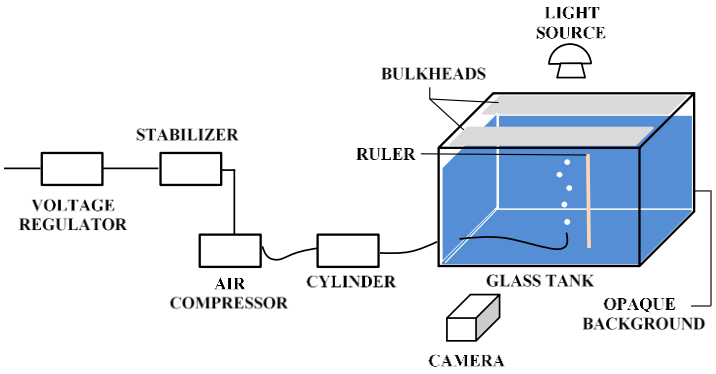

Fig. 1. Experimental schematics

In total, 21 tests were performed, at flow rate ranging from 21.1 mL/min to 234.4 mL/min and orifice inner diameter ranging from 1, 2 to 5 mm. All tests were based on the bubbles' chain regime; thus, the system had already reached equilibrium at the time the tests were performed (Figure 2).

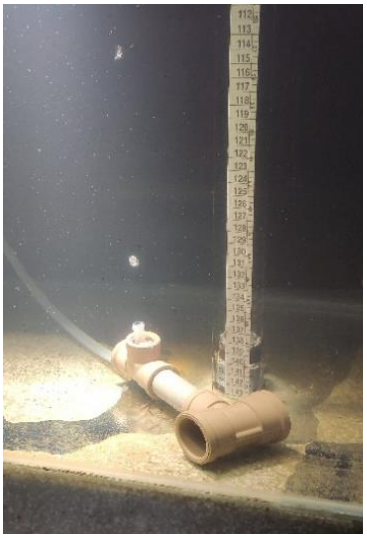

Fig. 2. Bubbles rising near the orifice (5 mm)

Test videos' duration ranged from 6 to 10 s; they were recorded at the rate of 240 frames per second (fps), and it resulted in a wide variety of bubbles per test. The camera had processing capacity of 1280 x 720 pixels in one frame; a source of light was positioned above the tank with two bulkheads in order to create a slit of light on the bubble axis. This procedure made the bubbles visually sharper and decreased the reflection of light. The background of the tank was covered with a frosted black and internally opaque material to avoid the emergence of shadows from the bubbles. A scale graduated at millimeter level was positioned parallel to the vertical axis to be used as reference in the videos (Figure 3).

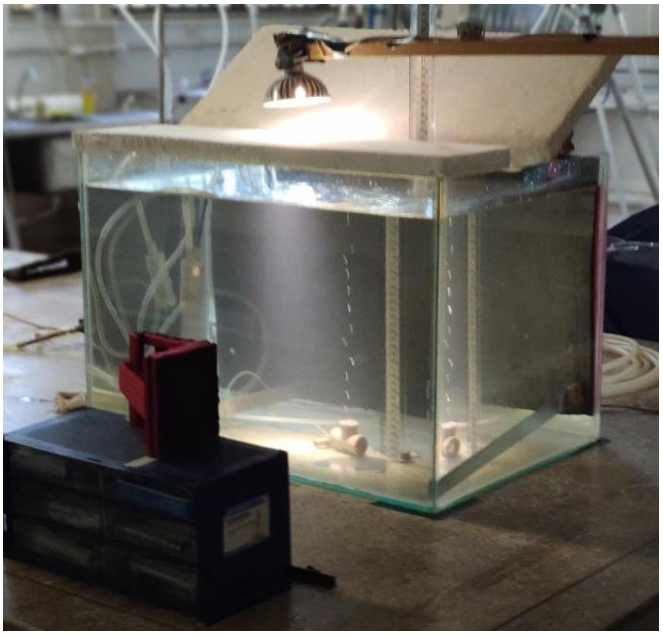

Fig. 3. Bubbles' chain in tests tank and lightning system

Air leak volume, V_{air}, was measured with a beaker, which was positioned inside the tank, with its opening facing downwards to enable collecting air bubbles. The time interval, Δt, was measured with the aid of a chronometer. Three air leak volume and time measurements were taken in each test.

The direct method was applied to determine the flow rate of the tests; in other words, the ratio between air leak volume and the time interval corresponding to the leak, as shown in the following equation:

$$Q = \frac{V_{air}}{\Delta t} \tag{2}$$

The number of air bubbles recorded in the videos, n_b, was counted during a certain time interval, Δt_c, and bubble emission frequency, f_e, was calculated through the following equation:

$$f_e = \frac{n_b}{\Delta t_c} \tag{3}$$

The volume of a leaked air bubble, V_b, was calculated based on flow rate and on emission frequency, by taking into consideration that bubbles have the same size, as shown in the following equation:

$$V_b = \frac{Q}{f_e} = \frac{V_{air}}{n_b} \tag{4}$$

Finally, the bubble equivalent diameter was found through the sphere volume equation, as shown earlier in Eq. (1).

Water specific gravity were measured with Digital Densimeter DMA 5000 (Anton-Paar) equipped with syringe injection in closed system. Water viscosity was measured with the aid of a manual Cannon-Fenske Viscometer Tube (Sigma-Aldrich). Air viscosity and surface tension of water and air were assumed from values validated in the technical literature (Table 5).

Table 5
Water properties

ρ (kg/m³)	μ (kg/m.s)	σ (N/m)
998	1.02×10^{-3}	0.072

2.2 Numerical Simulations

In addition to the experimental approach, Computational Fluid Dynamics (CFD) simulations were performed for comparison purposes. The numerical approach was also assessed as potential tool to help designing an automated subsea gas leakage monitoring system based on image analysis algorithms that can be used as data source for neural networks training [30]. The herein performed simulations and the related numerical parameters have replicated the experimental test conditions.

The unsteady incompressible viscous flow was modeled by mass and momentum conservation. Continuity and unsteady Reynolds-Averaged Navier-Stokes (RANS) equations were then satisfied in the fluid domain, as shown in the following equations:

$$\frac{\partial \underline{u_i}}{\partial x_i} = 0 \tag{5}$$

$$\rho \frac{\partial \underline{u_i}}{\partial t} + \rho \frac{\partial \underline{u_i} \underline{u_j}}{\partial x_j} = -\frac{\partial \underline{P}}{\partial x_i} + \frac{\partial}{\partial x_j}\left(\mu \frac{\partial \underline{u_i}}{\partial x_j} - \rho u'_i u'_j\right) + g_i + \sigma \tag{6}$$

Wherein, ρ is fluid density; $u_i = \left(\underline{u_i} + u'_i\right)$ is fluid velocity decomposition in mean and fluctuating velocities, respectively; $\underline{P}$ is mean dynamics pressure; μ is dynamics viscosity; σ is surface tension force at the two-phase interface; and i and j subscripts indicate the direction of an orthogonal axes-based system [30].

The classical κ-ε model was used to solve the turbulence closure issue [31], as shown in the following equations:

$$\frac{\partial(\rho k)}{\partial t} + \frac{\partial(\rho k \underline{v_i})}{\partial x_i} = \frac{\partial}{\partial x_j}\left(\frac{\mu_T}{\sigma_k}\frac{\partial k}{\partial x_i}\right) + 2\mu_T E_{ij}.E_{ij} - \rho\varepsilon \tag{7}$$

$$\frac{\partial(\rho \varepsilon)}{\partial t} + \frac{\partial(\rho \varepsilon \underline{u_i})}{\partial x_i} = \frac{\partial}{\partial x_j}\left(\frac{\mu_T}{\sigma_\varepsilon}\frac{\partial \varepsilon}{\partial x_i}\right) + 2\mu_T C_{1\varepsilon}\frac{\varepsilon}{k}E_{ij}.E_{ij} - \rho C_{2\varepsilon}\frac{\varepsilon^2}{k} \tag{8}$$

Wherein, k is turbulent kinetic energy; E_{ij} is the deformation rate of a given fluid element; and μ_T is turbulent viscosity, as shown in Eq. (10), Eq. (11) and Eq. (12), respectively. Moreover, ε is turbulent dissipation rate, and the adjustable constants used in the model are given by: C_μ = 0.09; σ_k = 1; σ_ε = 1.30; $C_{1\varepsilon}$ = 1.44; $C_{2\varepsilon}$ = 1.92.

$$\kappa = \left(\frac{1}{2}\left|\underline{u_i'}\right|^2\right) \tag{9}$$

$$E_{ij} = \frac{1}{2}\left(\frac{\partial \underline{u_i}}{\partial x_j} + \frac{\partial \underline{u_j}}{\partial x_i}\right) \tag{10}$$

$$\mu_T \left(= \rho C_\mu \frac{\kappa^2}{\varepsilon}\right) \tag{11}$$

The Volume of Fluid (VOF) method proposed by Hirt and Nichols [32] was applied to model the air-water interface. This method introduced the volume fraction approach, according to which, fluid properties at the interface are associated with both the contribution of each phase and with its individual properties. An additional transport equation for a given phase volume fraction must be included in the calculations to track the two-phase interface, as shown in the following equation:

$$\frac{\partial \alpha_q}{\partial t} + u_i \frac{\partial \alpha_q}{\partial x_i} = 0 \tag{12}$$

Wherein, α is the volume fraction of a given phase q: $\alpha_q = 0$, when the cell has no q phase inside it; $\alpha_q = 1$, when the cell is full of q phase; and $0 < \alpha_q < 1$, when there is interface in the cell.

The Continuum Surface Force (CSF) formulation proposed by Brackbill *et al.,* [33] was used for surface tension modelling. The Piecewise Linear Interface Construction (PLIC) scheme proposed by Youngs [34] was used for interface reconstruction, whereas pressure-velocity coupling was solved based on using the Pressure-Implicit with Splitting Operators (PISO) algorithm; PRESTO scheme was used for pressure discretization, whereas the second order upwind was used for momentum, turbulent kinetic energy and dissipation rate discretization purposes.

The finite volume method was applied to solve the partial differential equations in CFD commercial software ANSYS Fluent 2019, version 3. The 3D fluid domain (dimensions comprising 125 mm, in width; and 250 mm, in height) was discretized through 2.3 x 10^6 tetrahedral elements with mesh refinement near to the leakage orifice (Figure 4).

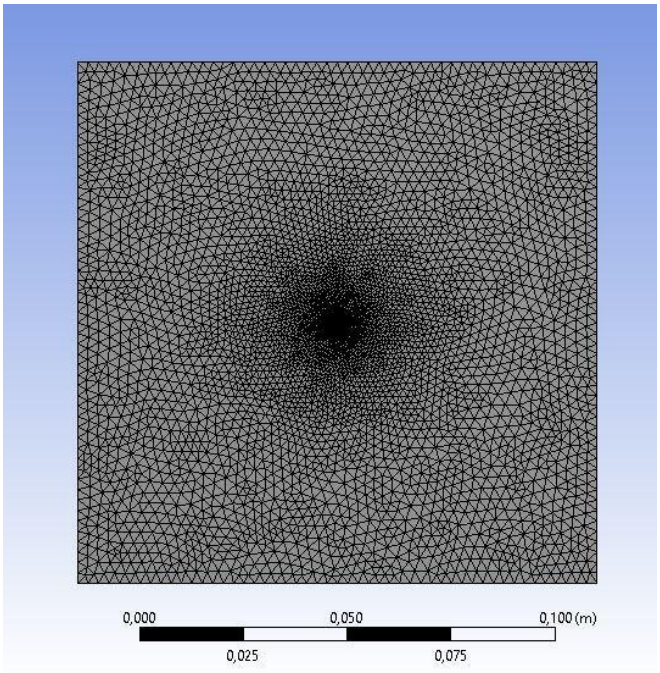

Fig. 4. Fluid domain discretization (bottom view)

A 0.5-ms time interval was set for several total simulation times. Zero shear wall stress was set in all boundaries to help mitigating its effect on the air bubble, except for the top, where a free-surface was used under pressurized condition to compensate the water hydrostatic pressure in the

experiments; and for the bottom, where the no-slip condition was applied. Air bubbles were released at the mid-bottom of the fluid domain at several velocities, based on using the same orifice's inner diameters used at the experimental model. All computations were carried out on a 64 bit, 3.4 GHz Intel Core i9-9900 processor with 16 Gb of RAM.

3. Results

Seven (7) flow rate values were proportionally distributed between the minimum and maximum flows found within each of the three inner diameters of the orifice (1, 2 and 5 mm). These limits were featured by the beginning of constant bubble formation and by the time right before plume formation. Each test refers to a different flow rate value; 21 tests were conducted, in total. Each flow value was calculated based on the mean recorded for the three measurements taken in the same test; it was done to help minimizing any likely variation in the system. Table 6 presents all inlet flow rates used in the experiments and their respective equivalent bubble diameters.

Table 6
Experimental results

Orifice's inner diameter (mm)	Q (mL/min)	d_e (mm)
1.0	21.1	4.1
	31.0	4.1
	54.1	4.4
	69.2	4.1
	82.9	4.6
	93.9	4.4
	101.2	4.5
2.0	25.2	4.8
	30.9	4.9
	46.4	4.5
	72.3	5.0
	95.6	5.3
	110.8	5.5
	153.2	5.9
5.0	30.0	6.4
	42.1	6.6
	69.0	7.0
	86.6	7.0
	131.9	7.5
	189.5	7.9
	234.4	8.2

Three (3) different flow rate values were used for each one of the three orifices' inner diameter, for numerical simulations purposes. Each simulation referred to a different flow rate value, and it resulted in 9 numerical simulations, in total. This process enabled a significant scenario to be compared to those of experimental tests. Table 7 presents the inlet flow rate and velocity ranges recorded for each orifice's inner diameter, as well as the bubble equivalent diameters.

It is possible seeing that the relative errors between experimental and numerical results increased, as orifice's inner diameter decreased, as well as good agreement for d_o = 5 mm and relatively large difference for d_o = 1 mm, mainly at higher velocities.

Table 7
Relation of numerical simulations results

Orifice's inner diameter (mm)	Q (mL/min)	d_e (mm)	u (m/s)
1.0	11.0	5.1	0.24
	32.0	5.6	0.68
	69.0	6.0	1.47
2.0	31.0	5.7	0.16
	72.0	6.1	0.38
	111.0	6.6	0.59
5.0	87.0	6.4	0.07
	132.0	6.9	0.11
	190.0	7.4	0.16

As previously mentioned, the comparison between numerical and experimental results has evidenced higher discrepancy in smaller orifices. In addition to the need of having a more refined mesh close to the orifice, orifice geometry simplification plays important role in helping properly modelling the surface tension effects on a critical region. Dietrich *et al.,* [35] have experimentally shown the effects of orifice shapes on bubble detachment volume, as well as observed that these effects decreased, as orifice diameter increased. This behaviour can be seen in the present results, which suggested that the simplified orifice shape in the numerical model can contribute to relative errors. Despite the quantitative differences observed for some cases, numerical results have shown physical coherence – i.e., bubble equivalent diameter increased, as gas flow rate increased at almost the same slope of those experimentally observed both in the present study and in the literature.

3.1 Experimental Comparison

Wang and Socolofsky [27] have investigated the motion of air bubbles continuously released from an orifice (4.0 mm, in diameter) into still water. Their experiment recorded bubble equivalent diameter ranging from 4.4 to 5.7 mm, based on bubble generation frequency ranging from 84 to 734 bubbles/min. Their experimental results were plotted along with those of the present study (Figure 5). The analysis of Q versus d_e has indicated increase in bubble equivalent diameter due to increase in the inner diameter of the orifice. It is also noteworthy that the recorded increased flow rate also contributed to higher bubble equivalent diameter values.

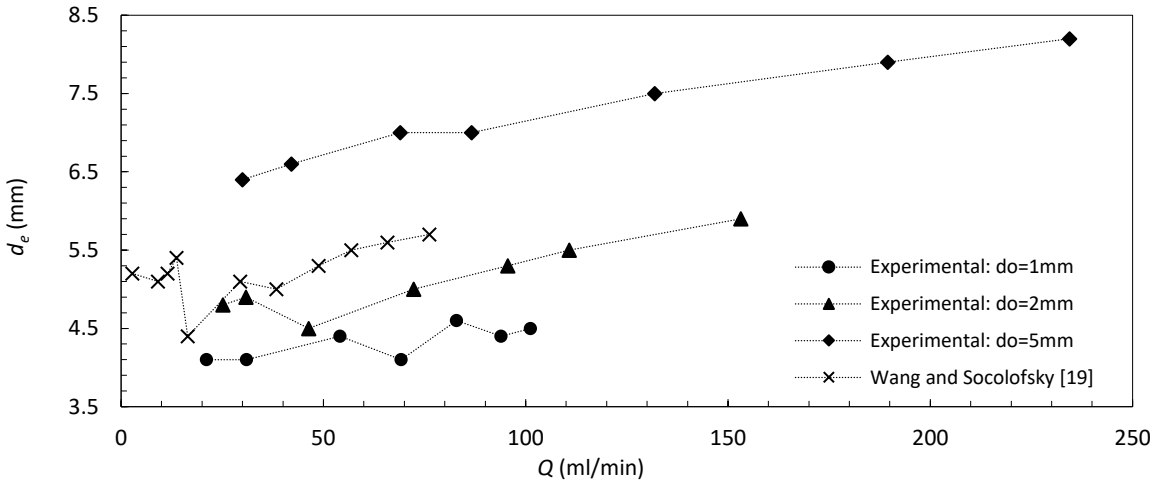

Fig. 5. Comparison d_e versus Q between experimental results and Wang and Socolofsky [27], for different d_o

It is remarkable how results in the present study are consistent to those recorded in Wang and Socolofsky's experimental tests, since linearity is observed in results as the orifice inner diameter increases. Furthermore, results recorded by the aforementioned authors for d_o = 4 mm are consistent with results recorded for d_o = 2 mm and d_o = 5 mm in the present study.

3.2 Analytical Comparison

Experimental and numerical results were also compared to the main analytical predictions available in the literature. These predictions were calculated based on analytical equations used by other authors, who were introduced at the beginning of the present article. These calculations used both fluid properties and experimental data of the present study. The mean value between each calculated d_e and the respective experimental value found in the current study was calculated for the analytical equation used by each author (Table 8).

Table 8
Deviation between experimental and numerical d_e and the authors' predictions

Correlation	Experimental percent average error (trust rating = 95%)	Numerical percent error (confidence interval = 95%)
Van Krevelen and Hoftjizer [11]	-25 ± 7.9	-37 ± 6.2
Davidson and Schuler [12]	-30 ± 7.3	-41 ± 5.8
Kumar and Kuloor [14]	-38 ± 6.5	-48 ± 5.2
Akita and Yoshida [15]	-2.2 ± 6.8	-15.3 ± 9.9
Gaddis and Vogelpohl [16]	-7.0 ± 2.4	-19.5 ± 5.1
Jamialahmadi [17]	-4.5 ± 2.4	-16.6 ± 5.3
Shi [10]	-15 ± 3.1	-25 ± 5.3
Xiao [26]	86 ± 12	65 ± 14

Studies conducted by Akita and Yoshida [15] and Jamialahmadi [17] were the ones that mostly agreed with results in the current study. Thus, they were selected to be compared to the present research, as well as to all bubble diameter results reported in both herein analyzed experimental and numerical cases. Results in the present study were plotted against the analytical predictions of the two selected authors, based on the orifice's inner diameter.

The best convergence recorded for the experimental results was observed at d_o = 1 mm (Figure 6a). The d_o = 2 mm has shown intermediate convergence; this result was closer to the one recorded by Jamialahmadi [17] and deviated from those recorded by Akita and Yoshida [15] for higher flows (Figure 6b). The d_o = 5 mm, in its turn, has shown lower compatibility between the two authors (Figure 6c). Despite the aforementioned distance, linearity similar to that recorded by Jamialahmadi [17] was evident.

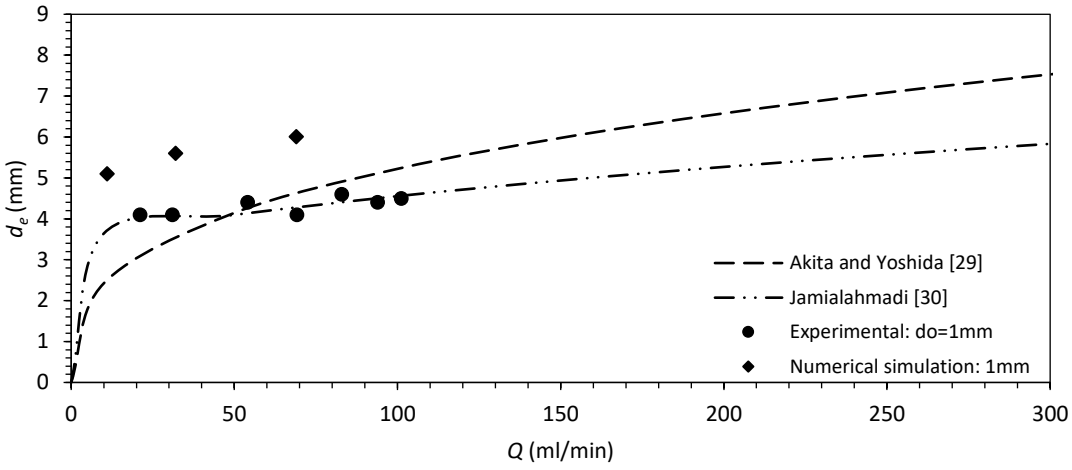

(a)

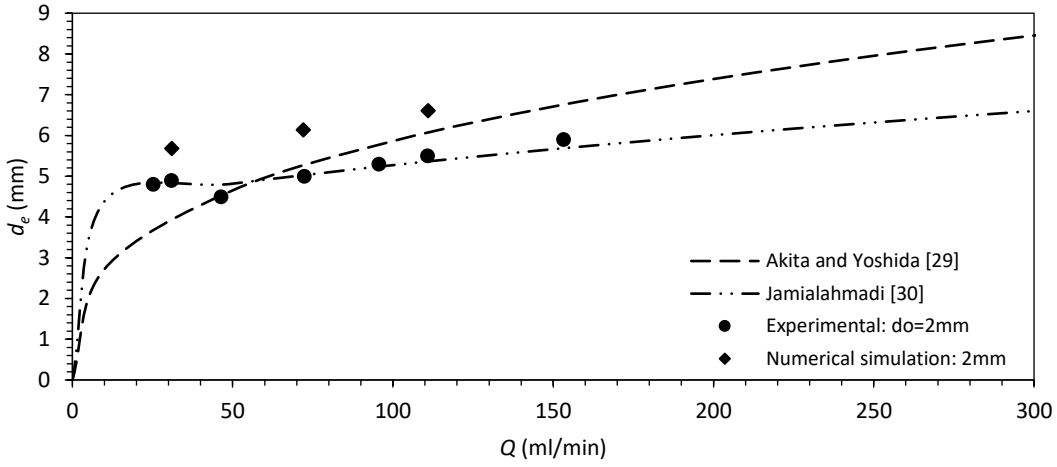

(b)

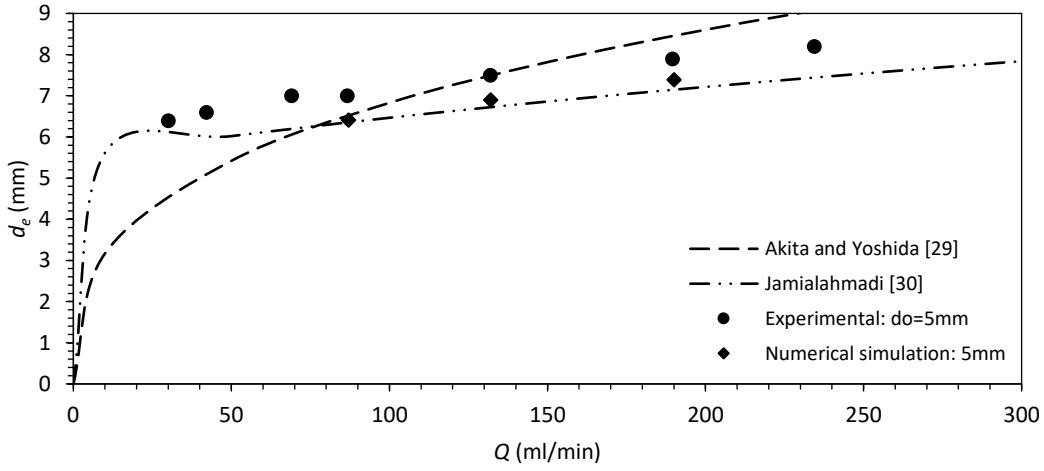

(c)

Fig. 6. Comparison of d_e versus Q between results in the current study and results by the main assessed authors, for (a) d_o = 1 mm, (b) d_o = 2 mm and (c) d_o = 5 mm

As previously discussed, the agreement between numerical and experimental results recorded for larger orifice's inner diameters has increased. Despite the distance in relation to d_e observed for both, d_o = 1 mm and d_o = 2 mm, the linearity similar to both, Jamialahmadi [17] and the experimental results, is notorious for the numerical results.

Results in the current study were consistent with those observed in the literature. Akita and Yoshida [15] recorded dispersion in calculated results higher than that observed by Jamialahmadi [17], a fact that justified Akita and Yoshida's longer distance from the experimental results. In addition, it is important emphasizing that Jamialahmadi [17] took into account fluids' properties. This factor provides greater credibility to validate results in the present study and enables conducting future studies with different fluids.

4. Conclusions

The herein performed numerical simulations presented relatively good agreement with experimental results, mainly for larger orifice diameters. However, in qualitative terms, results observed for all orifice diameters were in compliance with the experimentally observed ones - bubble equivalent diameter has increased, as the gas flow rate in the same slope also increased. It was possible seeing that the smaller the orifice's inner diameter, the higher the discrepancy between numerical and experimental results. This finding suggested the influence of orifice shape simplification on the observed results [35].

Thus, it is possible highlighting the validation of the herein performed experiments against the main analytical predictions and experimental data available in the literature. It is worth emphasizing that Wang and Socolofsky [27] were the authors whose results were the closest to the current ones, based on the use of the same fluid-fluid system. Therefore, experimental results have shown high compatibility to Wang and Socolofsky [27]: similar growth trend and proportional Q versus d_e relationship.

The compatibility of the present experimental results to Akita and Yoshida [15] and Jamialahmadi [17] models change as the inner diameter of the orifice increases. Overall, the 1 mm orifice presented the lowest compatibility of results, whereas the 5 mm orifice presented the best convergence level. Furthermore, Jamialahmadi [17] have shown better agreement when compared with the other analysed authors. It may have happened because the author took into account the physical properties of the analysed fluids.

Based on that, it is concluded that the experimental model developed in the present study could be validated by the main studies in the literature, in addition to showing good consistency with the present numerical model. It is therefore an important step in predicting the magnitude of leaks in structures located at great depths, where it is generally only possible to obtain information from images recorded by underwater vehicles. Measuring such leaks more accurately would reduce environmental damage and avoid higher costs for companies responsible for subsea structures.

Finally, future studies comprising extensive and detailed experiments and numerical simulations based on subsea temperature, salinity and pressure simulations should be conducted. In addition, once the correlation among flow rate, orifice inner diameter and bubble equivalent diameter was evidenced, it is important working with other relevant parameters such as terminal velocity and bubble trajectory.

Acknowledgement
The authors of the current article are grateful to Petrobras and ANP – National Petroleum Agency for providing the technical and financial support to develop the project titled "Development and application of fluid dynamic analysis techniques to quantify and evaluate subsea leaks based on images", which resulted in the present article.

References

[1] Chen, P., M. P. Duduković, and J. Sanyal. "Three-dimensional simulation of bubble column flows with bubble coalescence and breakup." *AIChE journal* 51, no. 3 (2005): 696-712. https://doi.org/10.1002/aic.10381

[2] Moys, M. H., J. Yianatos, and J. Larenas. "Measurement of particle loading on bubbles in the flotation process." *Minerals Engineering* 23, no. 2 (2010): 131-136. https://doi.org/10.1016/j.mineng.2009.11.004

[3] Yang, Zongbo, Jun Cheng, Richen Lin, Junhu Zhou, and Kefa Cen. "Improving microalgal growth with reduced diameters of aeration bubbles and enhanced mass transfer of solution in an oscillating flow field." *Bioresource Technology* 211 (2016): 429-434. https://doi.org/10.1016/j.biortech.2016.03.127

[4] Behr, Arno, Marc Becker, and Johannes Dostal. "Bubble-size distributions and interfacial areas in a jetloop reactor for multiphase catalysis." *Chemical engineering science* 64, no. 12 (2009): 2934-2940. https://doi.org/10.1016/j.ces.2009.03.031

[5] Huang, Jie and Saito, Takayuki. "Influences of gas–liquid interface contamination on bubble motions, bubble wakes, and instantaneous mass transfer", *Chemical Engineering Science* 157 (2017: 182-199. https://doi.org/10.1016/j.ces.2016.05.013

[6] Torregrosa, A. J., A. Broatch, P. Olmeda, and O. Cornejo. "A note on bubble sizes in subcooled flow boiling at low velocities in internal combustion engine-like conditions." *Journal of Applied Fluid Mechanics* 9, no. 5 (2016): 2321-2332. https://dx.doi.org/10.18869/acadpub.jafm.68.236.23211

[7] Krishna, R., and J. M. Van Baten. "Mass transfer in bubble columns." *Catalysis today* 79 (2003): 67-75. https://doi.org/10.1016/S0920-5861(03)00046-4

[8] Gupta, Puneet, Booncheng Ong, Muthanna H. Al-Dahhan, Milorad P. Dudukovic, and Bernard A. Toseland. "Hydrodynamics of churn turbulent bubble columns: gas–liquid recirculation and mechanistic modeling." *Catalysis today* 64, no. 3-4 (2001): 253-269. https://doi.org/10.1016/S0920-5861(00)00529-0

[9] Tate, Thomas. "XXX. On the magnitude of a drop of liquid formed under different circumstances." *The London, Edinburgh, and Dublin Philosophical Magazine and Journal of Science* 27, no. 181 (1864): 176-180. https://doi.org/10.1080/14786446408643645

[10] Shi, S. D. "Basic engineering of coal hydroliquefaction." (2012).

[11] VanKrevelen, D. W., and P. J. Hoftijzer. "Studies of gas-bubble formation-Calculation of interfacial area in bubble contactors." *Chemical Engineering Progress* 46, no. 1 (1950): 29-35.

[12] Davidson, J. F. "Bubble formation at an orifice in a viscous liquid." *Transactions of the Institution of Chemical Engineers* 38 (1960): 144-154.

[13] Davidson, J. F., D. Harrison, and R. Jackson. "Fluidized particles. Cambridge University Press, 1963. 155 pp. 35s." *Chemical Engineering Science* 19, no. 9 (1964): 701-701.

[14] Kumar, R., and N. K. Kuloor. "The formation of bubbles and drops." In *Advances in chemical engineering*, vol. 8, pp. 255-368. Academic Press, 1970. https://doi.org/10.1016/S0065-2377(08)60186-6

[15] Akita, Kiyomi, and Fumitake Yoshida. "Bubble size, interfacial area, and liquid-phase mass transfer coefficient in bubble columns." *Industrial & Engineering Chemistry Process Design and Development* 13, no. 1 (1974): 84-91.

[16] Gaddis, E. S., and A. J. C. E. S. Vogelpohl. "Bubble formation in quiescent liquids under constant flow conditions." *Chemical Engineering Science* 41, no. 1 (1986): 97-105. https://doi.org/10.1016/0009-2509(86)85202-2

[17] Jamialahmadi, M., M. R. Zehtaban, H. Müller-Steinhagen, A. Sarrafi, and J. M. Smith. "Study of bubble formation under constant flow conditions." *Chemical Engineering Research and Design* 79, no. 5 (2001): 523-532. https://doi.org/10.1205/02638760152424299

[18] Xiao, Hang, Shujun Geng, Aqiang Chen, Chao Yang, Fei Gao, Taobo He, and Qingshan Huang. "Bubble formation in continuous liquid phase under industrial jetting conditions." *Chemical Engineering Science* 200 (2019): 214-224. https://doi.org/10.1016/j.ces.2019.02.009

[19] Haberman, William L., and R. K. Morton. *An experimental investigation of the drag and shape of air bubbles rising in various liquids*. Washington, DC: David W. Taylor Model Basin, 1953.

[20] Marks, C. H. "Measurements of the terminal velocity of bubbles rising in a chain." (1973): 17-22. https://doi.org/10.1115/1.3446951

[21] Wu, Mingming, and Morteza Gharib. "Experimental studies on the shape and path of small air bubbles rising in clean water." *Physics of fluids* 14, no. 7 (2002): L49-L52. https://doi.org/10.1063/1.1485767

[22] Tomiyama, A., G. P. Celata, S. Hosokawa, and S. Yoshida. "Terminal velocity of single bubbles in surface tension force dominant regime." *International journal of multiphase flow* 28, no. 9 (2002): 1497-1519. https://doi.org/10.1016/S0301-9322(02)00032-0

[23] Shew, Woodrow L., Sebastien Poncet, and Jean-François Pinton. "Force measurements on rising bubbles." *Journal of Fluid Mechanics* 569 (2006): 51-60. https://doi.org/10.1017/S0022112006002928

[24] Melo, Fabiana Regina Grandeaux de. "Fluidodinâmica de esferas leves e bolhas em líquidos." (2007).
[25] Liu, Liu, Hongjie Yan, and Guojian Zhao. "Experimental studies on the shape and motion of air bubbles in viscous liquids." *Experimental Thermal and Fluid Science* 62 (2015): 109-121. https://doi.org/10.1016/j.expthermflusci.2014.11.018
[26] Sharaf, D. M., A. R. Premlata, Manoj Kumar Tripathi, Badarinath Karri, and Kirti Chandra Sahu. "Shapes and paths of an air bubble rising in quiescent liquids." *Physics of Fluids* 29, no. 12 (2017). https://doi.org/10.1063/1.5006726
[27] Wang, Binbin, and Scott A. Socolofsky. "On the bubble rise velocity of a continually released bubble chain in still water and with crossflow." *Physics of Fluids* 27, no. 10 (2015). https://doi.org/10.1063/1.4932176
[28] Raymond, F., and J-M. Rosant. "A numerical and experimental study of the terminal velocity and shape of bubbles in viscous liquids." *Chemical Engineering Science* 55, no. 5 (2000): 943-955. https://doi.org/10.1016/S0009-2509(99)00385-1
[29] Clift, R., J.R. Grace, and M.E. Weber. Bubbles, Drops and Particles, *Academic Press*, 1978.
[30] Caldas, Gustavo L. R., Thiago F. B. Bento, Roger M. Moreira, and Maurício B. de Souza Jr. (2021). "Detection of subsea gas leakages via computational fluid dynamics and convolutional neural networks", *International Congress of Mechanical Engineering*.
[31] Launder, B.E. and Spalding, D.B. (1974). "The numerical computation of turbulent flows", *Computer Methods in Applied Mechanics and Engineering* 3, no. 2 (1974): 269-289.
[32] Hirt, C.W. and Nichos, B.D. "Volume of fluid (VOF) method for the dynamics of free boundaries", *Journal of Computational Physics* 39, no. 1 (1981): 201-225. https://doi.org/10.1016/0021-9991(81)90145-5
[33] Brackbill, Jeremiah U., Douglas B. Kothe, and Charles Zemach. "A continuum method for modeling surface tension." *Journal of computational physics* 100, no. 2 (1992): 335-354. https://doi.org/10.1016/0021-9991(92)90240-Y
[34] Youngs, David L. "Time-dependent multi-material flow with large fluid distortion." *Numerical methods for fluid dynamics* (1982).
[35] Dietrich, Nicolas, Nadia Mayoufi, Souhil Poncin, and Huai-Zhi Li. "Experimental investigation of bubble and drop formation at submerged orifices." *Chemical Papers* 67 (2013): 313-325. https://doi.org/10.2478/s11696-012-0277-5